Journal of Materials Chemistry A

ROYAL SOCIETY OF CHEMISTRY

PAPER

View Article Online
View Journal | View Issue

Cite this: J. Mater. Chem. A, 2024, 12, 26772

Ozonolysis of regular and crosslinked lignin nanoparticles: closing the loop†

Alexandros E. Alexakis * and Mika H. Sipponen *

Received 2nd July 2024
Accepted 5th August 2024

DOI: 10.1039/d4ta04564e

rsc.li/materials-a

Crosslinked lignin nanoparticles have been developed to produce chemically robust grades suitable for demanding applications. However, their end-of-life degradation has remained elusive. In this work, we studied oxidative degradation of regular, non-covalently assembled LNPs and crosslinked hydroxymethylated LNPs (HLNPs). The results suggest that HLNPs degrade in the same fashion as regular LNPs through the transformation of aromatic rings into muconic acid moieties. This transformation was studied by UV-vis, ^{31}P-NMR, 2D-NMR and FTIR and it was found to be rapid within the first 120 min of ozonolysis. During ozonolysis, the LNPs degrade into smaller nanoparticles, as shown by SEM and DLS, until their ultimate degradation and conversion into acetals and small organic acids, supported by LC-MS data.

Introduction

The growing demand for environmentally friendly materials has spurred extensive research efforts to discover and develop renewable alternatives. To this end, in many parts of the world, a promising candidate and a source for a variety of biobased materials is wood.[1] Amongst the major components of wood and the most abundant natural aromatic macromolecule is lignin, which possesses excellent UV, thermal and chemical properties.[2–4] The primary source of lignin for materials applications is technical lignin from the pulp and paper industry, with potential availability of 10–20 Mt of kraft lignin annually.[5,6]

Lignin is used in numerous applications, ranging from polyurethanes to thermosets.[7,8] However, in most of them, the heterogeneity of lignin is an obstacle that is bypassed through fractionation or modification, which require large amounts of organic solvents and sometimes toxic chemicals. This is one of the reasons why lignin nanoparticles (LNPs) have gained interest. LNPs can be produced at mass yields exceeding 90%, have a well-defined spherical shape and high surface area, and are stabilized through electrostatic interactions emanating from the dissociated phenolic hydroxyl and carboxylic acid groups that decorate their surface.[9] The main challenge LNPs face is their stabilization under alkaline and acidic pH conditions. Due to their electrostatic stabilization, LNPs dissolve at alkaline pH, whereas they aggregate at acidic pH, facing challenges in terms of their functionalization in the dispersion state.[10,11] A way to tackle this challenge is through crosslinking by either oxidoreductive enzymes such as laccases[12] or by other chemical approaches.[4] Recently our group presented a preparation of robust hydroxymethylated LNPs (HLNPs) that were crosslinked through a hydrothermal approach.[13] These HLNPs show superior chemical stability under alkaline pH and in different organic solvents, including tetrahydrofuran and dimethylformamide, for more than 6 months. However, due to their chemical robustness, their environmental risks, including potential toxicity and degradation products, have become questionable.

Ozone has been used already from the 1910s as a decomposition agent targeting the aromatic rings present in lignin's structure, ultimately delignifying cellulosic fibres so as to obtain high quality paper products.[14] Since then, ozone treatment has been fully adapted in pulp mills during the bleaching process, reducing the chemical cost and improving the environmental impact.[15,16] Apart from the pulp and paper industry, ozone oxidation has shown great potential in treating pollutants derived from pharmaceutical and personal care products.[17] These waste streams have been identified as a serious threat to marine environments and human health.[18]

During ozonolysis, ozone attacks the carbons of the aromatic units of lignin primarily between positions 3 and 4, forming muconic acid structures.[19] In the literature, ozonolysis of kraft lignin has been investigated either in organic solvents such as ethanol, methanol or dioxane or in alkaline water, where the ozone dosage ranged between 3 and 15 g h^{-1}.[19–23] The resulting lignin has a lighter brown/yellowish colour with an increased number of carboxylic acids due to the reduction of double bonds and the transformation of the aromatic rings into muconic acids. This introduction of carboxylic acids on lignin has been thought to be a great starting point for further chemical modifications. For instance, ozonated enzymatic lignin was grafted onto poly(ethylene glycol) and exhibited improved emulsifying properties.[24] The active oxidizing species

Department of Materials and Environmental Chemistry, Stockholm University, 10691 Stockholm, Sweden. E-mail: alexandros.alexakis@mmk.su.se; mika.sipponen@mmk.su.se

† Electronic supplementary information (ESI) available. See DOI: https://doi.org/10.1039/d4ta04564e

in ozonolysis are ozone and its decomposition products, while in enzymatic biodegradation, they are phenoxy radicals from laccases and various radicals or oxidized metal ions from peroxidases. This study is the first to explore the ozonolysis of LNPs, whereas previous research has used laccases to modify LNPs instead of extensively degrading them.[25,26] Although there are no reports on treating LNPs with peroxidases, enzymatic degradation of lignin in soil has been reviewed elsewhere.[27]

In the present work, we used a low dosage of ozone (0.6 g h^{-1}) to study the degradation of conventional LNPs prepared from softwood kraft lignin alongside hydrothermally crosslinked hydroxymethylated HLNPs in water (Fig. 1a). We hypothesized that the ozone will react with the outer surface layer of the LNPs, dissolving water-soluble acidic moieties, hence reducing the scattering intensity of their dispersions and, upon extended ozonolysis, fully degrading them. Characterization of the ozonolysis products using FTIR, UV-vis, DLS, ^{31}P-NMR, 2D-NMR, LC-MS, and SEM provided both qualitative and quantitative evidence of the degradation pathways of the lignin particles. We envision that the results of this study will pave the way for the degradation of chemically robust LNPs, therefore addressing their potential environmental risk and closing the loop of these functional materials.

Experimental

Materials and methods

Materials. Softwood kraft lignin (SKL, BioPiva100 pine kraft lignin), sodium hydroxide (VWR) and acetone (Honeywell) were used as received. Hydroxymethylated lignin nanoparticles (HLNPs) crosslinked by the hydrothermal approach were described in our previous publication.[13] Briefly, HLNPs are prepared by the anti-solvent precipitation method of hydroxymethylated SKL, followed by a hydrothermal curing approach. The hydroxymethylation was performed at 85 °C and the hydrothermal cell was heated to 150 °C.

Preparation of LNPs. A detailed protocol can be found in previous publications.[4,13] Briefly, SKL was dissolved in one volume of a 3 : 1 (w/w) mixture of acetone : water and three volumes of water were added to precipitate the lignin, forming lignin nanoparticles (LNPs) that were evaporated under reduced pressure and subjected to dialysis against deionized water to remove the remaining acetone.

Ozonolysis of LNPs and HLNPs. In a typical experiment, 50 mL of an LNP dispersion (~4 g L^{-1}) were transferred into a 250 mL beaker. Then, the dispersion was purged with ozone, through a syringe, produced from an ozone generator at

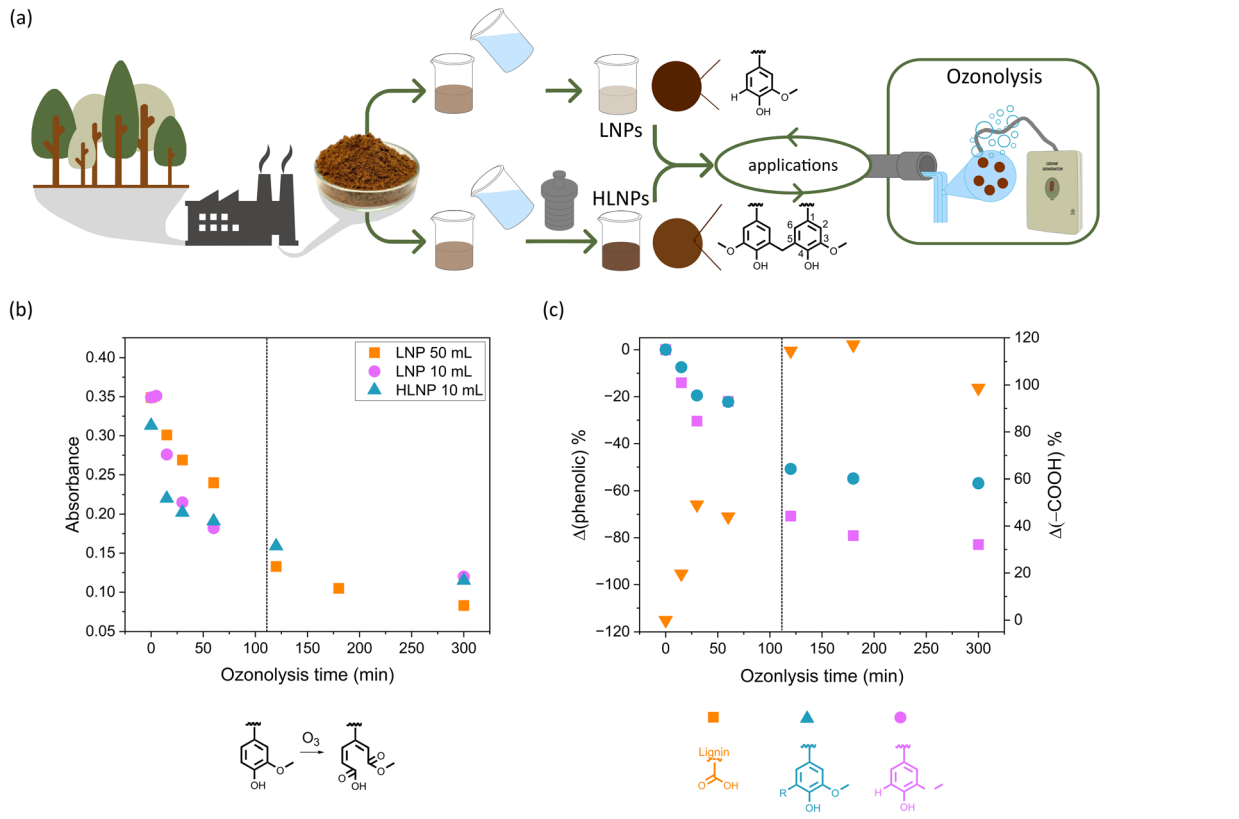

Fig. 1 Schematic representation of the preparation of lignin nanoparticles (LNPs) and hydroxymethylated and hydrothermally crosslinked LNPs (HLNPs) followed by their ozonation after their use (a). The absorbance peak at 284 nm obtained from the UV-vis spectrophotometer and plotted against ozonolysis time (b). Shown in the inlet label are the 50 mL LNP dispersion (orange squares), 10 mL LNP dispersion (pink circles) and 10 mL HLNP dispersion (cyan upward triangles). Percent change of hydroxyl groups of the LNP dispersion obtained from ^{31}P-NMR against ozonolysis time (c). The conversion of muconic acid moieties is shown below (b). The chemical groups of lignin plotted in (c) are shown below the graph; –COOH groups (orange downward triangles), condensed phenols (cyan circles) and non-condensed phenols (pink squares). The dashed line is used to indicate the time after which there are no significant changes to the investigated samples.

ambient temperature (~22 °C) (WUPYI2018, 220 V, 12 W, 50 Hz, 0.6 g h^{-1}). The pH was kept constant at ~3.4 by the addition of NaOH (0.1 M, aq.). The same experiment was repeated for a smaller volume, *i.e.*, 10 mL for LNPs and HLNPs.

Dynamic light scattering (DLS) and zeta potential measurements. The particle size and zeta potential were measured by using a Zetasizer Nano ZS90 instrument (Malvern Instruments Ltd, UK). The zeta potential measurements were conducted by using a dip cell probe. All samples were diluted to 0.1 g L^{-1} and all measurements were performed in triplicate and the reported values are the average values.

Fourier transform infrared (FTIR) spectroscopy. FTIR data were collected using a Varian 610-IR FTIR spectrometer. All samples were lyophilized prior to their analysis and they were analysed by 16 scans between 400 and 4000 cm^{-1}.

Nuclear magnetic resonance (NMR) spectroscopy. ^{31}P-NMR was conducted to quantify the different hydroxyl groups present on the LNPs before and after the ozonolysis. Briefly, lyophilized LNPs (30 mg) are phosphitylated with 2-chloro-4,4,5,5-tetramethyl-1,3,2-dioxaphospholane (0.9 mmol) in the presence of *N*-hydroxy-5-norbornene-2,3-dicarboxylic acid imine (0.010 mmol) as an internal standard and chromium(III) acetyl acetonate as a relaxation agent.[28] The ^{31}P-NMR experiments (256 scans, 10 s relaxation delay) were performed with a 90° pulse angle and inverse gated proton decoupling using a 400 MHz instrument (Bruker Avance). The solvent used was $CDCl_3$-d_3. 2D-NMR (Heteronuclear Single Quantum Coherence spectroscopy, HSQC) was conducted in a 500 MHz Bruker Avance I spectrometer equipped with a Bruker 5 mm BBI probe. The pulse sequence was hsqcetgpsi. The pulse length was 9.2 s with a D1 relaxation delay of 1.49 s and 44 scans were applied per sample (total 68 h per sample). The samples (~20 mg) were dissolved in DMSO-d_6.

Scanning electron microscopy (SEM). SEM imaging was conducted using a JSM-IT 800 (JEOL Ltd, Japan) and a secondary electron detector. The dispersions were diluted to a final concentration of 1 g L^{-1} and were spin coated onto hydrophilized silicon wafers (3000 rpm for 30 s).

UV-visible spectrophotometry. The UV-vis spectra of the ozonated LNP and HLNP dispersions were recorded using a GENESYS 150 (Thermo Scientific). The dispersions were diluted to 0.01 g L^{-1} prior to their characterization and the wavelength range was 200–700 nm.

Liquid chromatography-mass spectrometry (LC-MS). The measurement was conducted on a Waters Select Series Cyclic IMS system (Wilmslow, UK) with a time-of-flight mass analyser

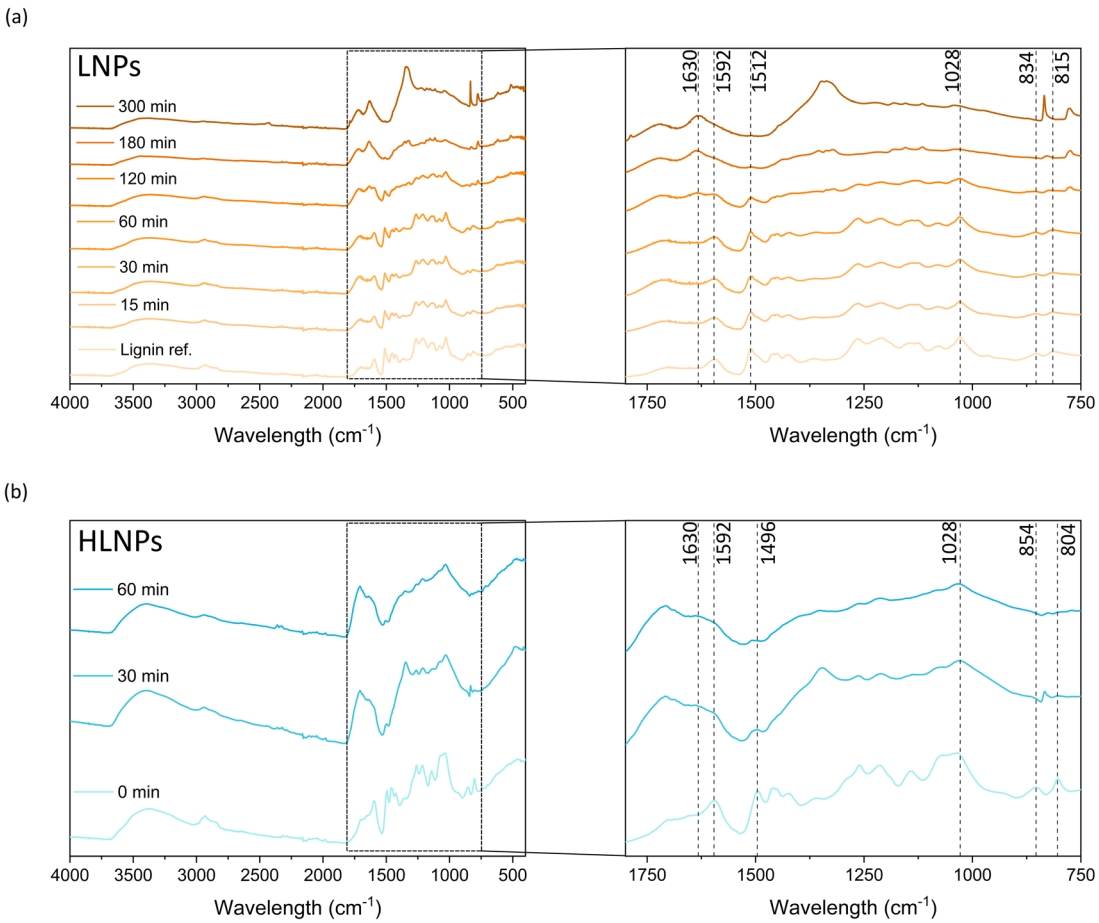

Fig. 2 FTIR spectra of lyophilized ozonated LNPs (a) and HLNPs (b). The dashed box is used to specify the region of interest which is shown in zoomed-in mode to the right of each graph. Vertical dashed lines indicate the wavelength that is discussed in the text.

at a mass resolution (mass to charge ratio (m/z) divided by the full peak width at half peak height) of 40 000. The samples and a blank were infused directly at a flow rate of 10 μL min^{-1}, each followed by infusion of leucine enkephalin for subsequent correction of the m/z measured. Spectra were acquired in both positive and negative ionization mode with the following source parameters: capillary voltage 2.3 kV (positive mode) or 2.0 kV (negative mode), cone voltage 40 V, source offset 10 V, source temperature 100 °C, desolvation temperature 300 °C, desolvation gas flow rate 800 L h^{-1}, cone gas flow rate 0 L h^{-1}, nebulizer gas pressure 6 bar. For ion mobility separation, a static T-wave height of 15 V and a T-wave velocity of 375 m s^{-1} was used and all ions were allowed to separate in one cycle. The time-of-flight mass analyser was set to scan within an m/z range from 50 to 2000 and a scan time of 1 s. After allowing the signal to stabilize, 60 scans were averaged for each infusion before comparing the drift time-resolved data at the different time points using Progenesis QI (version 3.0, Waters). A detailed description of data analysis can be found in the ESI.†

Results and discussion

The aim of this study was to investigate the ozonolysis of hydrothermally crosslinked hydroxymethylated lignin nanoparticles (HLNPs) and compare it with that of conventional LNPs. This way we aim to elucidate the possibility of oxidatively degrading these submicrometer particles either *via* chemical water treatment or under environmental conditions.

Influence of ozonolysis on chemical composition

Initially, the influence of the ozonated volume of the dispersion was investigated. Specifically, two different volumes of aqueous LNP dispersions (10 mL and 50 mL) were ozonated under constant stirring and ozone supply. Due to ozonolysis and therefore the generation of carboxylic acids, pH is expected to decrease (Fig. S1†).[23] This will affect the stability of the nanoparticles as it is known that LNPs aggregate at acidic pH.[10] Hence, pH was maintained at pH 3.4. Aliquots were taken at different time intervals and characterized by UV-vis at a diluted

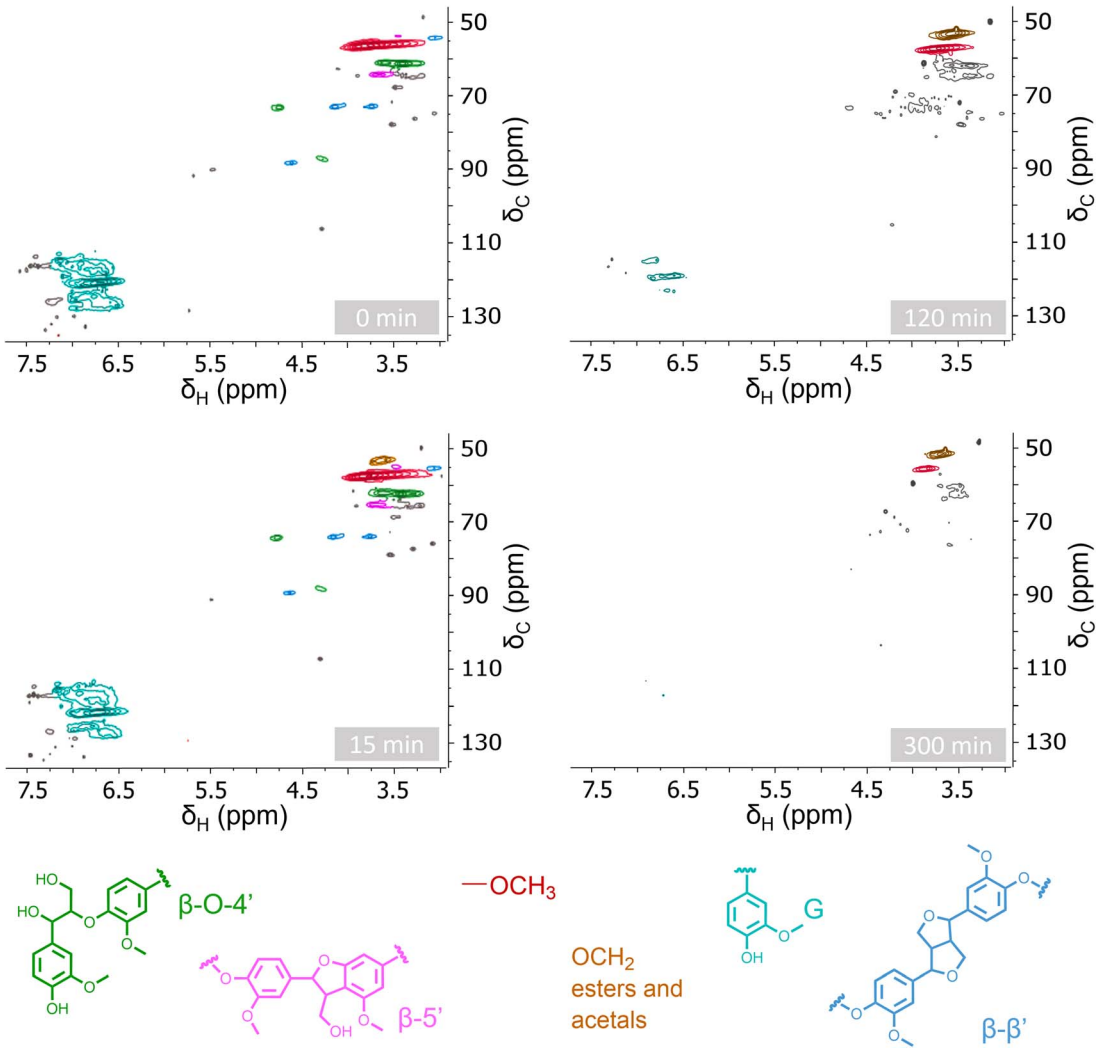

Fig. 3 HSQC-NMR of lyophilized ozonated LNP dispersions at 0 min, 15 min, 120 min and 300 min in DMSO-d_6. Some common lignin linkages are shown below the spectra following the respective colour coding.

concentration of 0.1 g L^{-1} and the aromatic absorbance peak at 284 nm was plotted against ozonolysis time (Fig. 1b). An exponential decrease of the peak was observed, for both volumetric cases. This suggests that ozone flow rate was sufficient to saturate the water phase irrespective of the reaction volume. This reduction of the aromatic peak at 284 nm is expected as ozone attacks the C3–C4 of the aromatic rings present in lignin, converting them into muconic acid moieties (see the chemical reaction below Fig. 1b).[19] Additionally, after 300 min of ozonolysis, the dry contents of the dispersions before and after ozonolysis were similar, suggesting that the same amount of oxygen is part of the final composition (Table S1†). Then, the same ozonolysis experiment was conducted for a 10 mL dispersion of HLNPs following the same trend as mentioned above (Fig. 1b). Although the HLNP dispersion was expected to exhibit a slower disappearance of the aromatic peak as it is a crosslinked system, there seems to be no difference when comparing it with the LNP dispersion. This observation indicates that (i) the breaking of the C3–C4 bonds of the aromatic ring is not hindered by the methylene bridge between the 5–5′ positions and (ii) the conversion of the aromatic ring into muconic acid occurs with the same rate as for a non-crosslinked LNP dispersion. According to studies performed on model lignin dimers, diarylmethane lignin compounds are equally sensitive to ozonolysis as biaryl compounds such as 5–5′ linkages, which are both altogether more sensitive than their monomeric counterparts (Fig. 1a).[19] This indicates that although the HLNPs are crosslinked through diarylmethane linkages, they can be degraded in a similar fashion to non-crosslinked LNPs.

Lyophilized aliquots from the ozonated LNP dispersion were investigated by ^{31}P-NMR (Fig. 1c and S2†). The trend previously observed by UV-vis, *i.e.*, reduction of the aromatic peak, was verified by the ^{31}P-NMR data. The reduction of both the condensed and non-condensed phenols (see the respective structures below Fig. 1c) is correlated with an increase of carboxylic acid groups which stem from the conversion of phenolic to muconic acid as reported elsewhere.[19,29] It must be noted that this rapid conversion takes place within the first 120 min of ozonolysis (marked by the dashed line in Fig. 1b and c), whereas thereafter no significant difference is observed. Due to the insolubility of the HLNPs, ^{31}P-NMR could not be performed. Lyophilized aliquots of the ozonated LNP dispersion were also characterized by FTIR (Fig. 2a). A general reduction of the characteristic lignin signals is observed upon increasing ozonolysis time.[14,30] Specifically, the intensity of the stretching band of $-CH_3/-CH_2$ at 2936 cm^{-1} and that of $-OCH_3$ at 2838–2840 cm^{-1} slightly decrease over time until they eventually disappear after 180 min. This indicates that the C4 of the aromatic ring is affected by ozonolysis and specifically from its transformation into muconic acid as described above. The intensities for the aromatic skeletal vibrations at 1512 and 1592 cm^{-1} also decrease over time until they either disappear or shift to 1630 cm^{-1}, respectively. This shift to higher wavelengths reportedly corresponds to muconic acid structures, *i.e.*, C=C

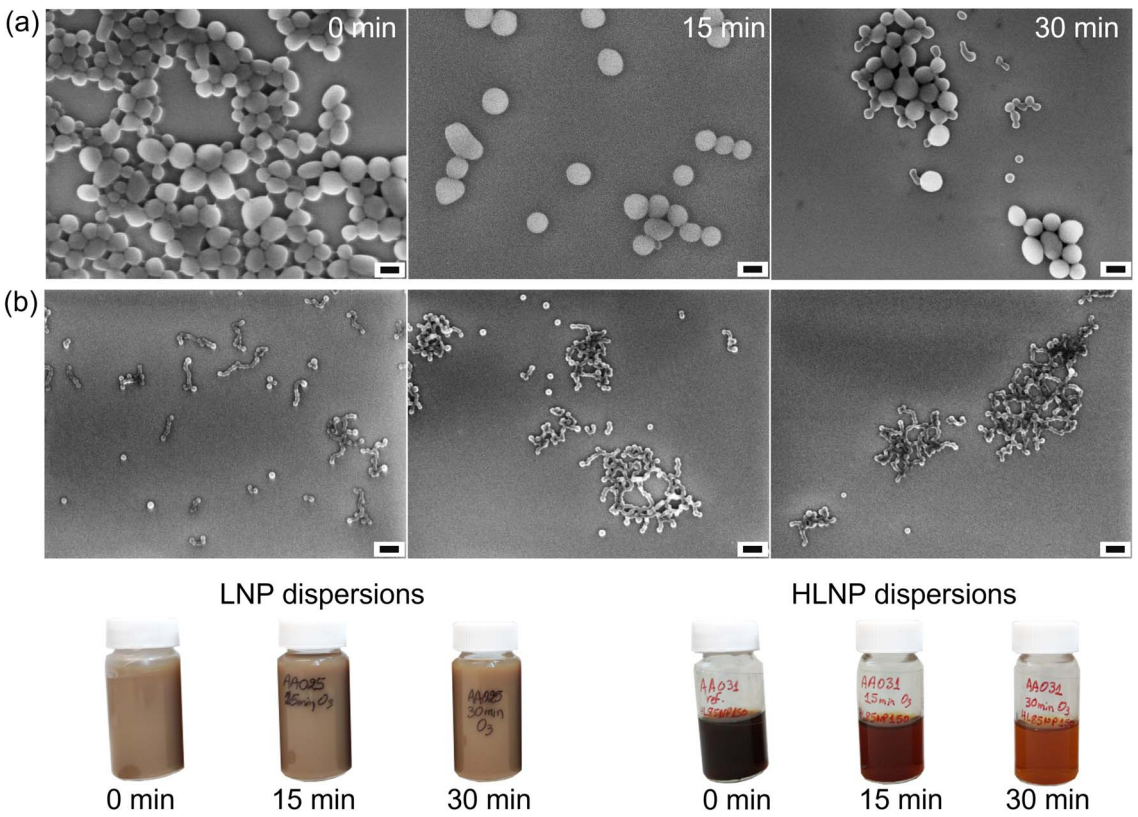

Fig. 4 SEM imaging of 0 min, 15 min, and 30 min ozonated LNPs (a) and HLNPs (b). Digital photos of the corresponding liquid ozonated dispersions are shown below the SEM images. The scale bar in all SEM images is 100 nm.

conjugated to the C=O group, further verifying the aforementioned trend.[31] The ether linkages between 1260 and 1028 cm^{-1} also decrease over time as ozone is known to have a high efficiency in cleaving ether bonds.[32] Additionally, the guaiacyl C=O stretching peaks at 1265 and 1210 cm^{-1} and the aromatic out-of-plane C–H deformation peak at 815 cm^{-1} decrease over time, where the latter also shifts to 834 cm^{-1}. When the same ozonolysis experiment was conducted for the HLNP dispersion, similar trends were observed for the aforementioned absorbance peaks (Fig. 2b). Another verification of the degradation of the phenolic structures comes from HSQC-NMR (Fig. 3). The large peaks between 6.4 and 7.8 ppm (δ_H) and 105 and 130 ppm (δ_C) corresponding to guaiacyl (G) units of the softwood kraft lignin that was used to prepare the LNPs disappeared after 120 min, verifying the ^{31}P-NMR and UV-vis data (Fig. 1b and c). The common lignin linkages such as β-O-4′, β-β′ and β-5′ also disappear after 120 min of ozonolysis, which follow the FTIR data (Fig. 2). The reduction of the intensity of the aromatic region gives rise to a new peak appearing right above the progressively reducing –OCH_3 peak at 3.46–3.76/52.05 ppm (δ_H/δ_C). This new peak is stable after 120 min of ozonolysis, and it corresponds to –OCH_2 esters and acetal groups, which could provide further proof of the muconic moiety.[22] It must be noted that due to the small amount of lyophilized material used and knowing the semi-quantitative nature of HSQC-NMR, only qualitative conclusions can be drawn.[33]

Influence of ozonolysis on morphology

The morphology of LNPs was investigated by SEM (Fig. 4 and S3†). All LNPs seem to maintain their spherical morphology until 30 min where smaller nanoparticles are shown which are the result of the degradation of larger ones (Fig. 4a). As shown in Fig. 5a, DLS identified some larger aggregated nanoparticles as well as a smaller fraction at lower D_H values as shown by the tail of the 60 min curve. Ozonated HLNP dispersions seem to be more robust in terms of morphology as their size according to SEM is not altered significantly (Fig. 4b). According to DLS (Fig. 5b), after 60 min, aggregated HLNPs are identified; however, this could not be verified by SEM as all the dispersions after 60 min of ozonolysis precipitated, indicating colloidal destabilization of the nanoparticles. The observed aggregation could be a result of the detachment of anionic lignin molecules rich in carboxylic acids from the nanoparticle surfaces or breakage of nanoparticles (inside-out) by electrostatic repulsions created by the transformation of aromatic rings into muconic acids. Furthermore, digital images of the dispersions after ozonolysis show a colour change, *i.e.*, lighter and transparent colour at higher ozonolysis times, which is a consequence of the degradation of the aromatic rings of lignin and the introduction of oxygen (Fig. 4 and S4†).[34]

Degradation products

To investigate the degradation products obtained from the ozonolysis of LNP and HLNP dispersions, LC-MS was used (Fig. 6). Due to the complex nature of the starting material, only qualitative analysis of these data was made. Additionally, to simplify

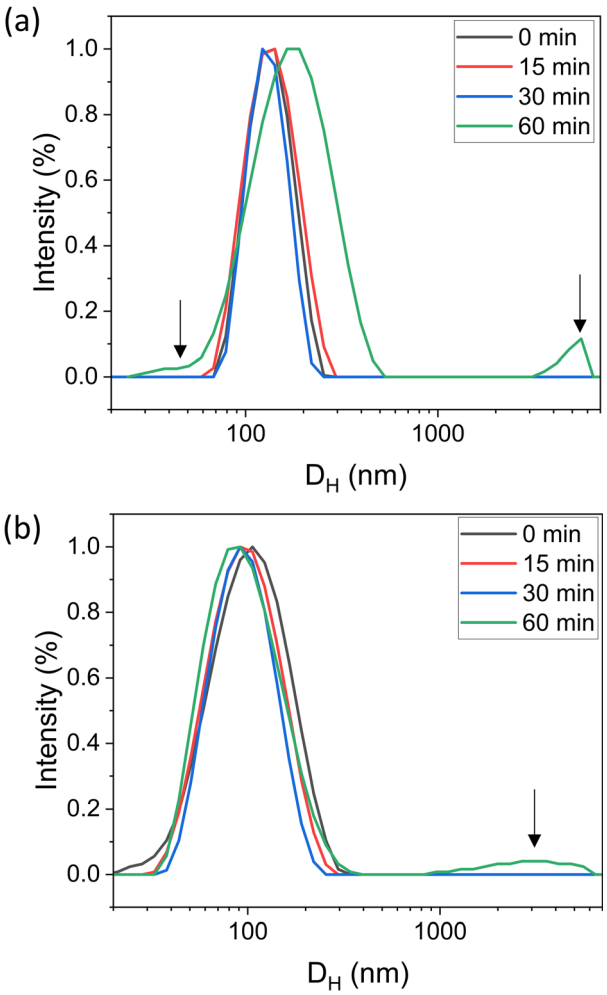

Fig. 5 Normalized particle size intensity of ozonated LNPs (a) and HLNPs (b) obtained from DLS. The arrows are used to highlight the regions of interest.

the data sets, the spectrograms are divided into 5 regions related to the number of repeating units calculated based on the assumption that a single monolignol has a molecular weight of approximately 180 g mol^{-1}. Functional groups that have a lone pair of electrons such as oxygen are expected to show up in the positive mode (Fig. 6) whereas phenolic and carboxylic acid groups should ionize better in the negative mode (Fig. S5†).

When comparing the number of peaks and the intensities of the two modes, it becomes very clear that the most interesting features are in the positive mode. In the case of LNPs, no significant differences can be seen in the first 15 min of ozonolysis (Fig. 6a). However, starting at 30 min, both the intensity and number of peaks in the regions related to monomers (1) and dimers (2) are increased. This becomes more apparent after 300 min of ozonolysis where more peaks are found in these regions, indicating the degradation of higher to lower molecular weight structures. These differences were more apparent for the HLNP dispersions, suggesting different degradation profiles of the investigated nanoparticle systems.

Most of the peaks of the intermediate molecular weight regions (2 and 3) show an initial increase of the intensity and

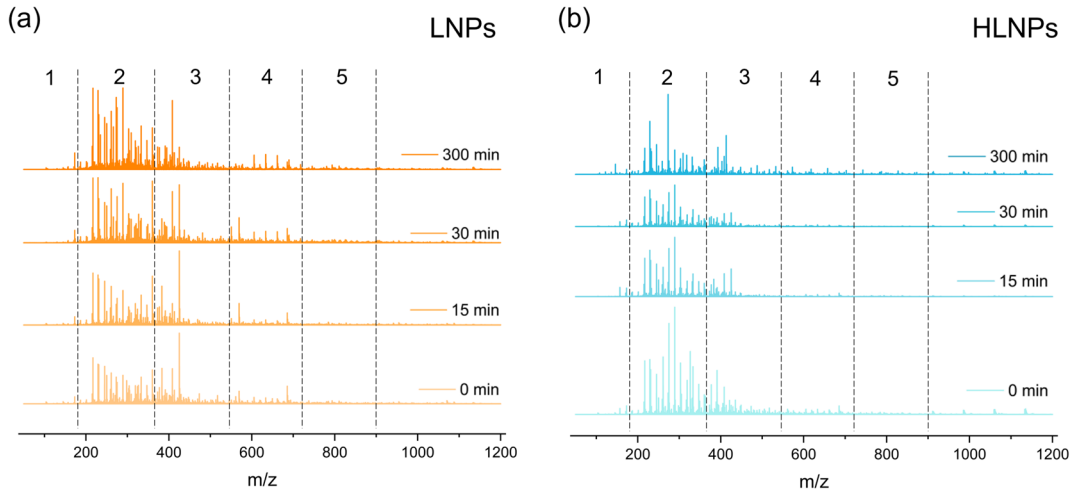

Fig. 6 LC-MS data for the ozonated LNPs (a) and HLNPs (b) from the positive mode. The dashed lines indicate the different regions where monomers (1), dimers (2), trimers (3), tetramers (4) and oligomers (5) can be found.

thereafter a decrease. By combining this observation with our conclusions mentioned above, we hypothesize that initially the molecular weight of the degraded structures is both increased, due to the addition of oxygen (as shown also in Table S1†), and decreased, due to the breaking of most likely ether bonds. Upon further ozonolysis these structures finally break down into smaller molecules giving rise to peaks in regions 1 and 2. According to the literature, ozonated lignin samples produce smaller organic molecules such as formic acid, acetic acid and oxalic acid as well as esters and acetals, the molecular weight of which coincides with regions 1 and 2.[21,22]

The overall morphological degradation of LNPs and HLNPs is shown schematically in Fig. 7, where by increasing the ozonolysis time, larger nanoparticles are broken down to smaller ones until their ultimate decomposition into organic acids at extensive ozonolysis times.

The degradation products presented in this study are similar to those of other studies where ozonolysis was used to degrade lignin. However, the reported studies were performed either under alkaline pH or in organic solvents, due to the insolubility of lignin, which influences altogether the final degradation products. For instance, the acetals that were obtained were functionalized with methyl or ethyl groups when the respective solvent was used.[22,23,35] Also, the fact that in our study lignin was used as nanoparticles reduced the time required to fully degrade lignin. Although fully soluble small organic molecules can find numerous applications, when aromaticity is desired to be retained then other oxidative degradation approaches related to electrochemistry or oxidation by using metals as catalysts need to be used.[36,37] Nonetheless, our results show that owing to their colloidal stability and large surface area to volume ratio the LNPs and HLNPs readily degrade in the presence of the reactive oxygen species generated during ozonolysis.

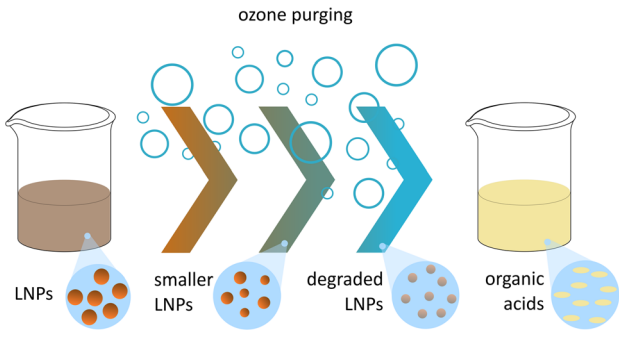

Fig. 7 Schematic representation of the morphological mechanism that takes place during the ozonolysis of LNPs. The arrow indicates the increase of ozonolysis time.

Conclusions

In this work, we studied the ozonolysis of regular and crosslinked LNPs. It was verified that for both investigated cases of particles ozone attacked the C3–C4 aromatic carbon creating muconic acid groups. This resulted in the reduction of the colour intensity of the dispersions as well as the reduction of the particle size by either the dissociation of carboxylic acid-rich lignin molecules from their surfaces or breakage of nanoparticles by intraparticle electrostatic repulsions. Additionally, it was shown that simultaneous addition of oxygen on lignin, breaking of ether linkages and, by extension, degradation of lignin polymers into smaller monomers or dimers promote the degradation of the lignin nanoparticles. Although other oxidative degradation approaches might result in the retention of the aromatic nature of lignin, ozonolysis results in small organic molecules with functionalities that are highly dependent on the solution environment. The results of this study prove that chemically robust LNPs such as the hydroxymethylated and hydrothermally crosslinked LNPs (HLNPs) undergo degradation to a similar extent compared to the regular supramolecular aggregates present in LNPs.

Data availability

The data supporting this article have been included as part of the ESI.†

Author contributions

Conceptualization (A. E. A., M. H. S.), data curation (A. E. A.), formal analysis (A. E. A.), funding acquisition (M. H. S.), investigation (A. E. A.), methodology (A. E. A., M. H. S.), project administration (A. E. A., M. H. S.), resources (M. H. S.), supervision (M. H. S.), validation (A. E. A.), visualization (A. E. A., M. H. S.), writing – original draft (A. E. A.), writing – review & editing (M. H. S.).

Conflicts of interest

There are no conflicts to declare.

Acknowledgements

Authors acknowledge the Swedish Foundation for Strategic Research (SSF) for financial support (SSF-FFL8 project SUSLIG, grant number FFL21-0006). We thank Dr Mohammad Morsali for providing a sample of HLNPs and Dr Claudia Möckel for technical assistance with the LC-MS investigation.

References

1 C. Montanari, P. Olsén and L. A. Berglund, *Front. Chem.*, 2021, **9**, 682883.
2 S. Sen, S. Patil and D. S. Argyropoulos, *Green Chem.*, 2015, **17**, 4862–4887.
3 M. H. Tran, D.-P. Phan and E. Y. Lee, *Green Chem.*, 2021, **23**, 4633–4646.
4 T. Zou, M. H. Sipponen, A. Henn and M. Österberg, *ACS Nano*, 2021, **15**, 4811–4823.
5 L. Dessbesell, M. Paleologou, M. Leitch, R. Pulkki and C. Charles) Xu, *Renewable Sustainable Energy Rev.*, 2020, **123**, 109768.
6 B. L. Tardy, E. Lizundia, C. Guizani, M. Hakkarainen and M. H. Sipponen, *Mater. Today*, 2023, **65**, 122–132.
7 A. Moreno and M. H. Sipponen, *Mater. Horiz.*, 2020, **7**, 2237–2257.
8 M. Fazeli, S. Mukherjee, H. Baniasadi, R. Abidnejad, M. Mujtaba, J. Lipponen, J. Seppälä and O. J. Rojas, *Green Chem.*, 2024, **26**, 593–630.
9 M. Österberg, M. H. Sipponen, B. D. Mattos and O. J. Rojas, *Green Chem.*, 2020, **22**, 2712–2733.
10 A. Moreno, J. Liu, M. Morsali and M. H. Sipponen, in *Micro and Nanolignin in Aqueous Dispersions and Polymers*, Elsevier, 2022, pp. 385–431.
11 R. Grappa, V. Venezia, L. Basta, M. L. Alfieri, L. Panzella, M. Verrillo, B. Silvestri, M. Commodo, G. Luciani and A. Costantini, *ACS Sustainable Chem. Eng.*, 2024, **12**, 10653–10664.
12 M.-L. Mattinen, J. J. Valle-Delgado, T. Leskinen, T. Anttila, G. Riviere, M. Sipponen, A. Paananen, K. Lintinen, M. Kostiainen and M. Österberg, *Enzyme Microb. Technol.*, 2018, **111**, 48–56.
13 M. Morsali, A. Moreno, A. Loukovitou, I. Pylypchuk and M. H. Sipponen, *Biomacromolecules*, 2022, **23**, 4597–4606.
14 X. Du, S. Wu, T. Li, Y. Yin and J. Zhou, *Fuel Process. Technol.*, 2022, **231**, 107232.
15 J.-C. Hostachy, *Tappi J.*, 2010, **9**, 16–23.
16 T. Miyanishi, *Jpn. TAPPI J.*, 2018, **72**, 427–434.
17 J. Jiao, Y. Li, Q. Song, L. Wang, T. Luo, C. Gao, L. Liu and S. Yang, *Materials*, 2022, **15**, 8152.
18 A. K. Thakur, R. Kumar, A. Kumar, R. Shankar, N. A. Khan, K. N. Gupta, M. Ram and R. K. Arya, *J. Water Proc. Eng.*, 2023, **54**, 103977.
19 H. Kaneko, S. Hosoya, K. Iiyama and J. Nakano, *J. Wood Chem. Technol.*, 1983, **3**, 399–411.
20 M. Ragnar, T. Eriksson, T. Reitberger and P. Brandt, *Holzforschung*, 1999, **53**, 423–428.
21 M. B. Figueirêdo, P. J. Deuss, R. H. Venderbosch and H. J. Heeres, *ACS Sustainable Chem. Eng.*, 2019, **7**, 4755–4765.
22 M. B. Figueirêdo, H. J. Heeres and P. J. Deuss, *Sustainable Energy Fuels*, 2020, **4**, 265–276.
23 O. Musl, M. Holzlechner, S. Winklehner, G. Gübitz, A. Potthast, T. Rosenau and S. Böhmdorfer, *ACS Sustainable Chem. Eng.*, 2019, **7**, 15163–15172.
24 C. Shi, S. Zhang, W. Wang, R. J. Linhardt and A. J. Ragauskas, *ACS Sustainable Chem. Eng.*, 2020, **8**, 22–28.
25 P. Figueiredo, D. Morais De Carvalho, M. H. Lahtinen, K. S. Hilden and K. S. Mikkonen, *Sustainable Mater. Technol.*, 2023, **37**, e00677.
26 L. Wang, L. Tan, L. Hu, X. Wang, R. Koppolu, T. Tirri, B. Van Bochove, P. Ihalainen, L. S. Seleenmary Sobhanadhas, J. V. Seppälä, S. Willför, M. Toivakka and C. Xu, *ACS Sustainable Chem. Eng.*, 2021, **9**, 8770–8782.
27 R. Datta, A. Kelkar, D. Baraniya, A. Molaei, A. Moulick, R. Meena and P. Formanek, *Sustainability*, 2017, **9**, 1163.
28 X. Meng, C. Crestini, H. Ben, N. Hao, Y. Pu, A. J. Ragauskas and D. S. Argyropoulos, *Nat. Protoc.*, 2019, **14**, 2627–2647.
29 B. Ferron, J. P. Croué and M. Doré, *Ozone: Sci. Eng.*, 1995, **17**, 687–699.
30 M. V. Bule, A. H. Gao, B. Hiscox and S. Chen, *J. Agric. Food Chem.*, 2013, **61**, 3916–3925.
31 P. Widsten, B. Hortling and K. Poppius-Levlin, *Holzforschung*, 2004, **58**, 363–368.
32 C. S. Osorio-González, K. Hegde, S. K. Brar, P. Vezina, D. Gilbert and A. Avalos-Ramírez, *Bioresour. Technol.*, 2020, **313**, 123638.
33 I. Sapouna, A. E. Alexakis, E. Malmström and L. S. McKee, *Ind. Crops Prod.*, 2023, **206**, 117660.
34 J. Wang, Y. Deng, Y. Qian, X. Qiu, Y. Ren and D. Yang, *Green Chem.*, 2016, **18**, 695–699.
35 M. B. Figueirêdo, F. W. Keij, A. Hommes, P. J. Deuss, R. H. Venderbosch, J. Yue and H. J. Heeres, *ACS Sustainable Chem. Eng.*, 2019, **7**, 18384–18394.
36 O. Y. Abdelaziz, K. Ravi, F. Mittermeier, S. Meier, A. Riisager, G. Lidén and C. P. Hulteberg, *ACS Sustainable Chem. Eng.*, 2019, **7**, 11640–11652.
37 N. Di Fidio, J. W. Timmermans, C. Antonetti, A. M. Raspolli Galletti, R. J. A. Gosselink, R. J. M. Bisselink and T. M. Slaghek, *New J. Chem.*, 2021, **45**, 9647–9657.